

# Metal Capping Layer Effects on Electromigration Failure Phenomena of Plasma Etched Copper Lines

To cite this article: Jia Quan Su et al 2020 ECS J. Solid State Sci. Technol. 9 104009

View the <u>article online</u> for updates and enhancements.





# Metal Capping Layer Effects on Electromigration Failure Phenomena of Plasma Etched Copper Lines

Jia Quan Su,\* Mingqian Li, and Yue Kuo\*\*, to

Thin Film Nano & Microelectronics Research Lab, Texas A&M University, College Station, Texas 77843-3122, United States of America

The electromigration failure phenomena of plasma etched copper lines on glass substrates with a titanium tungsten or molybdenum capping layer were studied. The failure of the line showed as the abrupt increase of the line resistance, which corresponded to the drastic change of the temperature. The surface color of the copper line also changed in the failure process. For the uncapped copper line, the color change was due to the surface oxidation at the raised temperature. For the capped line, the color change was contributed by the additional copper component diffused from the bulk copper film due to the raise of the temperature, which enhanced voids formation and shortened the failure time. Under the same current density condition, the copper diffusion into the titanium tungsten capping layer was less serious than that into the molybdenum capping layer, which was the reason of the longer lifetime of the former lines. This research confirms that the capping layer material is critical to the lifetime of the copper line.

© 2020 The Electrochemical Society ("ECS"). Published on behalf of ECS by IOP Publishing Limited. [DOI: 10.1149/2162-8777/abbb71]

Manuscript submitted July 14, 2020; revised manuscript received September 20, 2020. Published November 2, 2020. This was paper 1255 presented at the Atlanta, Georgia, Meeting of the Society, October 13–17, 2019.

Copper (Cu) is a popular interconnect material in ultra large scale integrated circuits (ULSICs), large-area thin film transistor (TFT) arrays, and other electronic products due to advantages of high conductivity, negligible hillocks formation, and high resistance to electromigration (EM). <sup>1–3</sup> Conventionally, the chemical-mechanical polishing (CMP) method is used to prepare Cu fine lines in ICs. <sup>3,4</sup> However, it involves complicated process steps that require environmentally unfriendly chemicals, e.g., strong oxidants, surfactants, and nanoparticles. In addition, the endpoint of the process is difficult to determine and the dishing phenomenon is often observed. <sup>5–7</sup> Furthermore, the CMP method is not applicable to the fabrication of large-area TFT arrays because the glass surface is not as flat as the wafer surface is.

Plasma etching has been widely used in preparing aluminum (Al) fine lines with well-controlled profiles and critical dimension (CD's).  $^{8-12}$  However, Cu cannot be etched with the conventional plasma etching method because Cu halides have very low vapor pressures below 500 °C.  $^{13}$  The Kuo's group first reported a novel plasma-based Cu etch process that is composed of two steps: a Cl or Br plasma-Cu reaction step that converts the Cu thin film into a porous halide compound layer at a high rate and the subsequent HCl solution dipping step that dissolves the halide compound instantaneously.  $^{14-18}$  The complete process can be done at room temperature. This process has been successfully used in fabricating 0.3  $\mu$  Cu patterns, BiCMOS chips, TFTs with complete Cu electrodes, and 15-inch TFT LCDs.  $^{18-21}$  Later on, it was reported that copper chloride could also be removed with the hydrogen plasma.  $^{22}$  However, the hydrogen plasma process has to be carried out at a low temperature, i.e., 10 °C, and the reaction rate is very low.

The reliability of a metal line is commonly evaluated by the electromigration (EM) method in which a very large current is passed through the line to accelerate the breakage process. <sup>23</sup> There was no report on the EM study of the plasma-etched Cu line until the first paper published by Liu and Kuo. <sup>24</sup> The Cu line width and length can affect the EM lifetime. For example, the wide line has a shorter lifetime than the narrow line because of the former's larger number of grain joints that function as flux divergence sites to enhance void formation. <sup>25</sup>

A barrier layer is usually added to the Cu line to enhance its adhesion to the substrate. For the Cu line, the barrier layer not only enhances the adhesion to the substrate but also prevents its diffusion to the substrate and adjacent layers. Titanium tungsten (TiW) and molybdenum (Mo) are common barrier materials for the Cu layer. 25–28 They are easily etched with plasma processes. 8,29,30 addition, Cu is subject to oxidize in air either at room temperature or at the high temperature, which could lower the electrical conductivity and reduce the lifetime, 31-33 the addition of a capping layer could prevent it from occurrence. There are reports that CoWP and CoWB can be good capping materials for the CMP prepared Cu <sup>36</sup> However, they are not common materials in semiconductor devices with limited information on their thermal properties or dry etching capability. And since the CMP Cu line is surrounded by the dielectric material and the plasma etched Cu line is free standing, their EM failure mechanisms may be different. Theoretically, for the CMP process, the Cu line is formed in the dielectric trench. The EM induced high temperature may affect the mechanical stress of the surrounding dielectric layer and at the interface. On the other hand, for the plasma etched Cu line, the surrounding dielectric is formed after the line is formed. The temperature effect on the adjacent dielectric film and at the Cu/ dielectric interface, e.g., stress and current flow along the interface, in these two types of structures may be different. More study is required to compare the reliability of CMP and dry etching prepared Cu lines with various types of capping layer materials. In this work, authors investigated the metal capping layer effect on the plasmaetched Cu lines. The electrical and physical changes of the Cu line during EM stresses were monitored. The failure mechanism of the line is discussed.

# **Experimental**

Sample preparation.—Two types of tri-layer Cu stacks, i.e., TiW (10 nm)/Cu (280 nm)/TiW (10 nm) and Mo (25 nm)/Cu (280 nm)/Mo (25 nm), were sputter deposited on a pre-cleaned Corning 1737 glass in one pump down without breaking the vacuum. The Cu stacks with individual layer thickness been listed are shown in Fig. 1. The TiW thin film was deposited from a Ti/W (10%/90% wt.) target at 75 W, 5 mTorr in Ar for 15 min. The Mo film was deposited at 100 W, 5 mTorr in Ar for 10 min. The Cu film was deposited at 80 W, 10 mTorr in Ar for 180 min. The samples were patterned into 4-probe configurations using a mask aligner (Quintel Q-4000). <sup>24,25</sup> The TiW capping and barrier layers were etched under the same condition of CF<sub>4</sub> 10 sccm at 60 mTorr, and 600 W for 2 min. The Mo barrier and capping layers were etched under the same condition of CF<sub>4</sub>/O<sub>2</sub> 10/10 sccm at 60 mTorr, and 600 W for 2 min. After the capping layer was etched off, the Cu film was exposed to the CF<sub>4</sub>/HCl (5/20 sccm) plasma at 70 mTorr, 600 W for 2 min. The exposed Cu film was

<sup>\*</sup>Electrochemical Society Student Member.

<sup>\*\*</sup>Electrochemical Society Fellow.

<sup>&</sup>lt;sup>z</sup>E-mail: yuekuo@tamu.edu

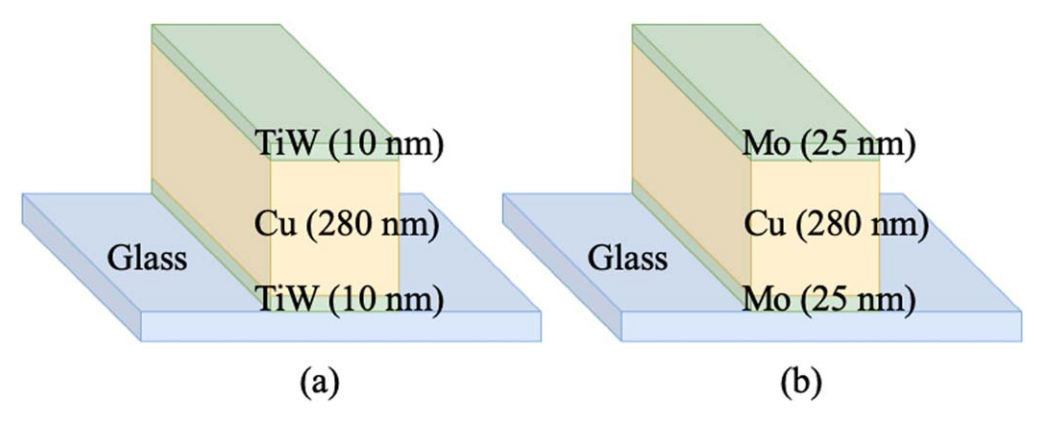


Figure 1. Cross-sectional views of (a) TiW/Cu/TiW and (b) Mo/Cu/Mo stacks.

completely converted into  $\text{CuCl}_{\text{x}}^{14-18}$  Subsequently, the sample was removed from the plasma reactor and immersed in a  $\text{HCl/H}_2\text{O}$  (1:8 v/v) solution for 1 min to completely dissolve the  $\text{CuCl}_{\text{x}}$  compound. Then the barrier layer was etched off with the plasma process. The photoresist layer was stripped with the AZ 400 T Stripper. For the comparison purpose, samples without the capping layer were also prepared. Before the plasma exposure of the Cu film, the sample was dipped in a diluted HCl solution (HCl: $\text{H}_2\text{O} = 1:4 \text{ v/v}$ ) to remove the surface native oxide. The plasma-Cu reaction was carried out in a parallel plate reactor (PlasmaTherm 700 C) operated at the reactive ion etching (RIE) mode.

*EM tests and Cu line temperature estimation.*—Samples were prepared into 2 μm, 10 μm, and 30 μm widths for the EM stress on a probe station (Signatone S-1160). The chuck temperature was controlled by a heat exchanger. The EM stress current density (*J*), which was fixed between  $2.57 \times 10^5$  and  $6.00 \times 10^6$  Amp cm<sup>-2</sup>, was supplied by an Agilent E3645A DC power supply and controlled with a Labview program. The barrier and capping layers are much thinner than that of the bulk Cu layer. In addition, the resistivities of the barrier and capping layers, i.e.,  $7 \times 10^{-5} \Omega \cdot \text{cm}$  for TiW and  $5.34 \times 10^{-6} \Omega \cdot \text{cm}$  for Mo, are larger than that of Cu, i.e.,  $1.68 \times 10^{-6} \Omega \cdot \text{cm}$ . Therefore, the currents flowing through the barrier and capping layers are negligible compared with that through the bulk Cu layer. The line resistance vs stress time (*R-t*) curve was recorded. The color and shape of the Cu line were also monitored.

The temperature of the Cu line during EM stress was estimated by modifying the JEDEC standard guidelines of JESD33-B. <sup>41</sup> This calculation method was applied to estimate the line temperature since it is difficult to directly measure the temperature of Cu lines with small geometry, e.g.,  $10~\mu m$  wide. In the original JEDEC standard guidelines, the temperature was calculated assuming the fixed initial line temperature and resistance. In this study, the Joule heat generated by the passage of the current through the Cu line did not dissipate effectively because the glass substrate had a low thermal conductivity. Assuming the adiabatic condition, Joule heat generated at stage i, i.e., time  $t_i$ , was conserved and used in the calculation of the line temperature at the beginning of the i+1, i.e., time  $t_{i+1}$ , stage. Then, the line temperature at stage i, i.e.,  $T_i$ , could be estimated from parameters in stage i-1 using the following equation.

$$T_{i} = \frac{R(T_{i}) - R(T_{i-1})}{R(T_{ref}) \times TCR(T_{ref})} + T_{i-1}$$
[1]

where  $R(T_i)$  is the resistance at temperature  $T_i$ ,  $R(T_{i-1})$  is the resistance at temperature  $T_{i-1}$ ,  $R(T_{ref})$  is the resistance at the reference temperature  $T_{ref}$ , i.e., 20 °C, and  $TCR(T_{ref})$  is the temperature coefficient of resistance at  $T_{ref}$ . The following equation was used to calibrate the  $TCR(T_{ref})$  value.

$$TCR(T_{ref}) = \frac{1}{R(T_{ref})} \times \frac{\Delta R}{\Delta T}$$
 [2]

where  $\Delta R$  is the resistance difference and  $\Delta T$  is the temperature difference.

According to Eq. 1, the temperature increases linearly with the line resistance. However, it was observed that when the temperature exceeded 230 °C, the deviation of temperature from linearity was non-negligible. <sup>41</sup> The calibrated temperature  $T_{cal}$  could be estimated by multiplying the originally calculated temperature  $T_i$  with the correction factor  $F_{corr}(T_i)$  using the following equations.

$$F_{corr}(T_i) = 1.0167 - 8.39751 \times 10^{-5} \times T_i$$
  
- 3.74768 × 10<sup>-8</sup> ×  $T_i^2$  [3]

$$T_{cal} = F_{corr}(T_i) \times T_i$$
 [4]

The calculated temperature may be different from the actual line temperature if the heat loss through the glass substrate is non-negligible. In addition, the change of the line temperature was estimated from the change of the resistance. Mechanisms of material damages during electromigration, e.g., change of morphology or formation of new voids, are important to the temperature change. A temperature measurement instrument for the small dimension sample, e.g., an IR microscope, may be used to verify the simulation result on the Cu fine line.

#### **Results and Discussion**

**Diffusion of Cu atoms to capping layers.**—The physical appearance of the capped Cu line changed after the EM stress. Figure 2 shows the TiW/Cu/TiW line surfaces (a) before and (b) after stress at  $J=1.39\times10^6$  Amp cm<sup>-2</sup> for 3 min. These images were taken using an optical microscope under the white light (Nikon Crescent 150) illumination. The original light purple color changed to the beige color after the stress. The similar color change was observed previously,<sup>37</sup> which could be contributed by the change of the light reflection from the TiW capping layer.

The surface chemical states of the TiW capping layer before and after the EM stress were characterized with the X-ray photoelectron spectroscopy (XPS). Figure 3 shows the Cu 2p peaks of the TiW layer (a) before and (b) after EM stress at  $J=1.39\times 10^6$  Amp cm<sup>-2</sup> for 5 min. The Cu peaks can be decomposed into Cu(0)+Cu(I) and Cu(II) subpeaks, i.e., Cu 2p<sub>3/2</sub> binding energies (BE's) of 932.61 eV and 933.57 eV as well as Cu 2p<sub>1/2</sub> BE's of Cu(0)+Cu(I) and Cu(II) are 952.36 eV and 953.32 eV, respectively. <sup>42–47</sup> The Cu(0) and Cu(I) peaks are too close to separate. <sup>42–47</sup> The satellite peaks at around BE 943 eV and 963 eV belong to CuO, which are shake-up peaks that occur when outgoing photoelectrons interact with valence electrons. <sup>43</sup> Table I lists the Cu atomic ratios calculated from the Cu

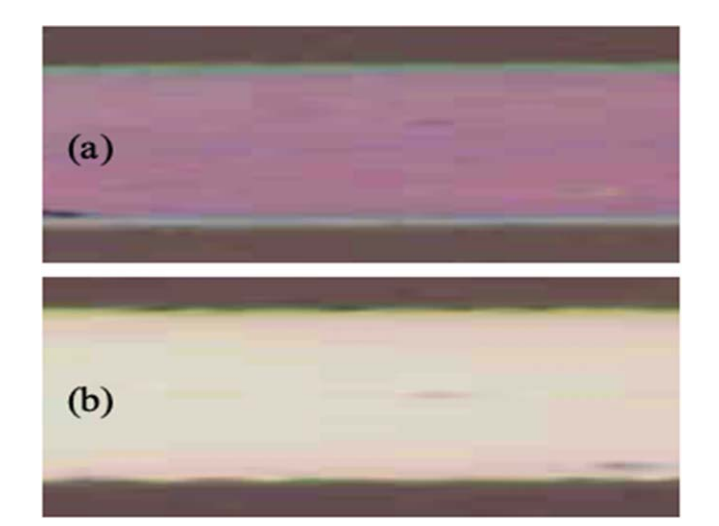
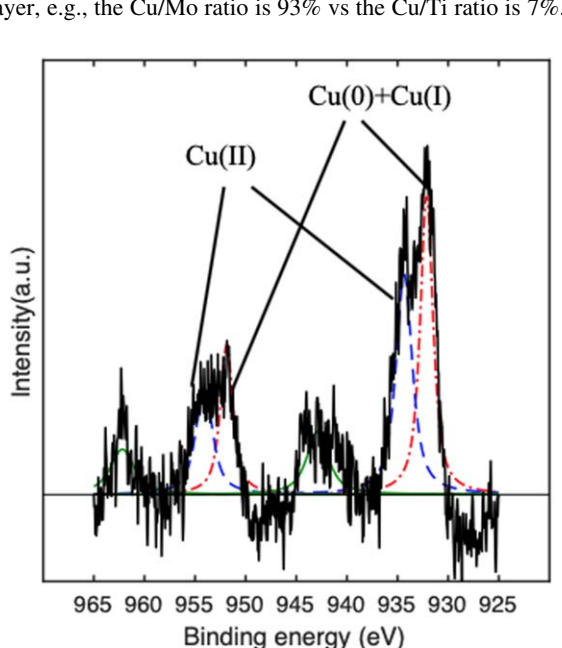


**Figure 2.** Surfaces of 30  $\mu$ m width TiW/Cu/TiW lines (a) before EM stress and (b) after 3 min current stress at  $J = 1.39 \times 10^6$  Amp cm<sup>-2</sup>.

 $2p_{3/2}$  peak. The total Cu to Ti ratio (Cu/Ti ratio) in the TiW capping layer increased by 7% after the EM stress. Since the Ti amount in the TiW is fixed independent of the EM stress, the Cu/Ti ratio increase is due to the diffusion of Cu atoms from the bulk Cu layer during the Joule heating.  $^{48-52}$  In addition, after the stress, the Cu(II)/total Cu ratio decreased from 0.49 to 0.39 and the [Cu(0)+Cu(I)]/total Cu ratio increased from 0.51 to 0.61. This can be explained by the partial oxidation of the diffused Cu atoms in the TiW capping layer at the raised temperature.

Figure 4 shows the Cu peaks in the Mo capping layers (a) before and (b) after the EM stress at  $J=7.71\times10^5$  Amp cm<sup>-2</sup> for 6 min. The Cu peaks can be split into subpeaks corresponding to Cu(0)+Cu (I) and Cu(II) bonds similar to those in the TiW capping layer. Table II lists ratios of Cu components of different chemical states summarized from Fig. 4. After the EM stress, Cu atoms were diffused from the bulk Cu film into the Mo capping layer and some of which were oxidized into Cu<sub>2</sub>O or CuO. However, the amount of Cu atoms in the Mo capping layer is larger than that in the TiW capping layer, e.g., the Cu/Mo ratio is 93% vs the Cu/Ti ratio is 7%.



(a)

Table I. Components in TiW capping layers before and after EM stress.

Component (area ratio)	Before	After
[Cu(0) + Cu(I)]/total Cu	0.51	0.61
Cu(II)/total Cu	0.49	0.39
Cu/Ti	0.28	0.30

The excessive loss of Cu atoms from the Cu bulk layer to the Mo capping layer under the high current stress condition may accelerate the formation of voids and therefore, shorten its EM lifetime. Under the high current stress condition, Cu atoms could diffuse into both the barrier and capping layers. In this study, we only focus the discussion on the capping layer effect.

Changes of temperature and resistance with stress time.—The change of line resistance with the EM stress time is a good reference in understanding the line failure process. Figure 5a shows R-t curves of the TiW/Cu and TiW/Cu/TiW lines at three different stress current densities, i.e.,  $J = 2.1 \times 10^6$ ,  $2.6 \times 10^6$  and  $3.6 \times 10^6$  Amp cm $^{-2}$ , separately. Each curve can be divided into 3 regions: first, the resistance increases slightly with time; second, the resistance increases at a higher rate; third, the resistance increases drastically and eventually reaches the broken point. The line broken process starts from voids formation with subsequent growth in size and number.  $^{23-25,37,53,54}$  Voids could be formed from Cu diffusion through multiple pathways, e.g., through surface, grain boundaries, capping layer/Cu interface, dislocations in the bulk film, etc.  $^{23-25}$ ,  $^{37,53,54}$  For the uncapped Cu, the surface diffusion is critical to the

<sup>37,33,54</sup> For the uncapped Cu, the surface diffusion is critical to the electromigration phenomena. The change of the line resistance with the stress time is contributed by all above factors. The large current accelerated this process and therefore, shortened the line broken time. <sup>55</sup> The addition of the TiW capping layer increased both the line resistance and the temperature during the EM stress. This is consistent with the result of Fig. 3 that the formation of voids was accelerated by the loss of Cu atoms from the bulk Cu layer to the capping layer.

The temperature change during the EM stress process demonstrated the Joule heating effect on the line failure. Figure 5b shows

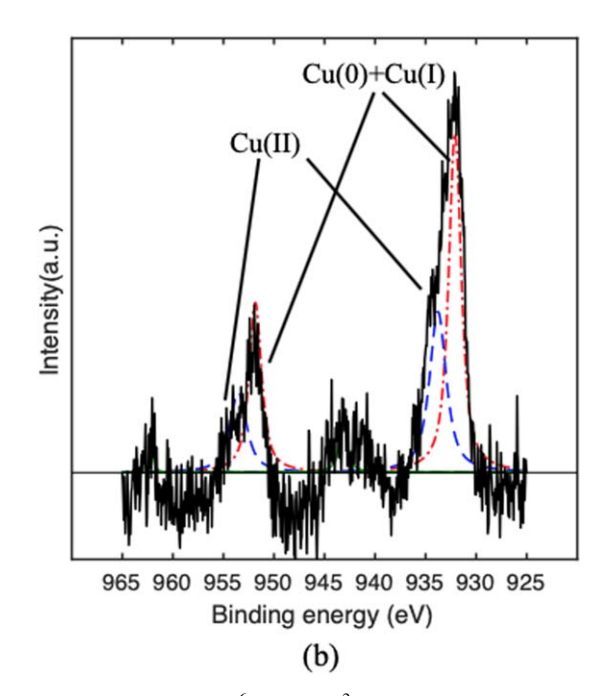
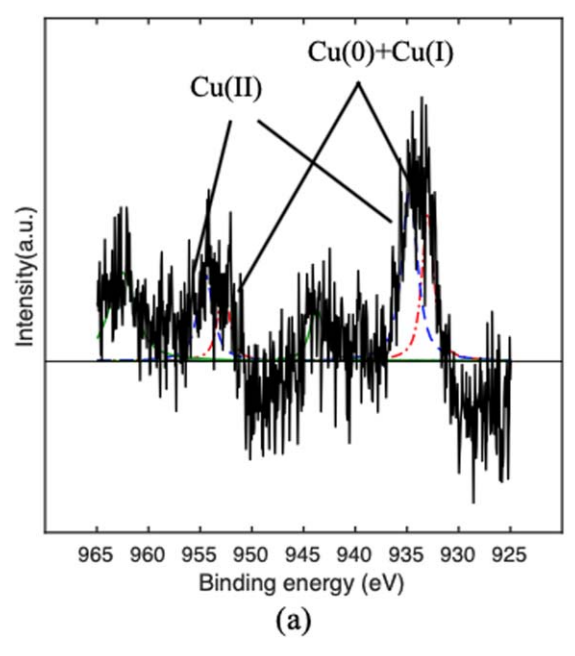


Figure 3. XPS Cu 2p peaks of TiW/Cu/TiW surfaces (a) before and (b) after EM stress at  $J = 1.39 \times 10^6$  Amp cm<sup>-2</sup> for 5 min.



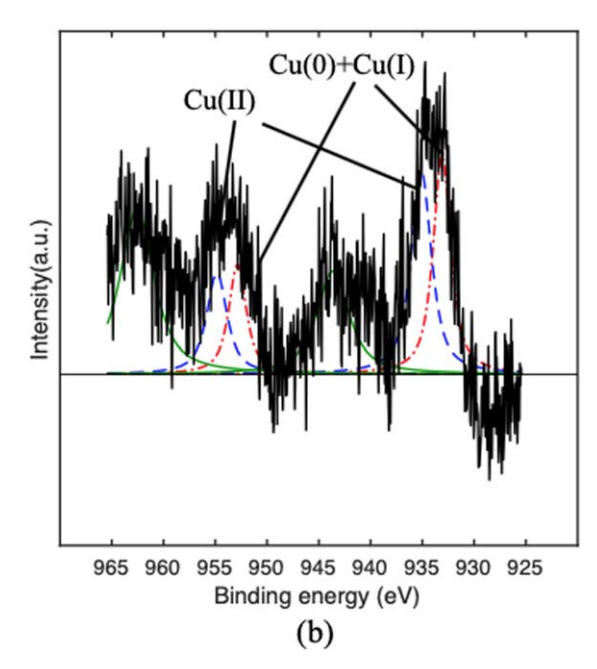


Figure 4. XPS Cu 2p peaks of Mo/Cu/Mo surfaces (a) before and (b) after EM stress at  $J = 7.71 \times 10^5$  Amp cm<sup>-2</sup> for 6 min.

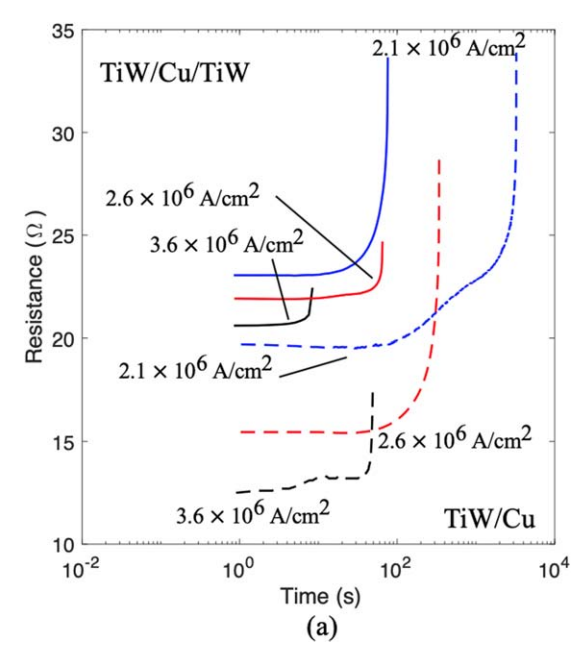
Table II. Components in Mo capping layers before and after EM stress.

Component (area ratio)	Before	After
[Cu(0) + Cu(I)]/total Cu	0.39	0.48
Cu(II)/total Cu	0.61	0.52
Cu/Mo	0.82	1.58

the temperature-time (T-t) curves corresponding to Fig. 5a curves. Similar to the R-t curve, the T-t curve is composed of 3 stages, i.e., slow, medium, and drastic raise of temperature, separately. Also, since the temperature increase is caused by Joule heating, the longer

the stress time is, the higher the temperature becomes. <sup>56</sup> The temperature of the TiW/Cu line stressed at  $J=2.1\times10^6$  Amp cm<sup>-2</sup> is estimated to be above 200 °C shortly before the broken point. The high temperature increased the mass flux rate at the joint of Cu grains, which facilitated the void formation and eventually the breakage of the line. <sup>53</sup> The diffusion of Cu atoms to the capping layer at the high temperature further enhanced the process.

Figure 6 shows (a) R-t and (b) T-t curves of Mo/Cu and Mo/Cu/Mo lines stressed at three different current densities, i.e.,  $J=7.71\times10^5$ ,  $9.00\times10^5$ , and  $1.03\times10^6$  Amp cm $^{-2}$ , separately. The trends of increases of resistance and temperature with the EM stress time are similar to those of the TiW/Cu and TiW/Cu/TiW lines. The resistance and temperature of the Mo/Cu/Mo lines are larger than those of the Mo/Cu lines. For example, the temperature of the Mo/Cu line stressed at  $J=7.71\times10^5$  Amp cm $^{-2}$  was higher than



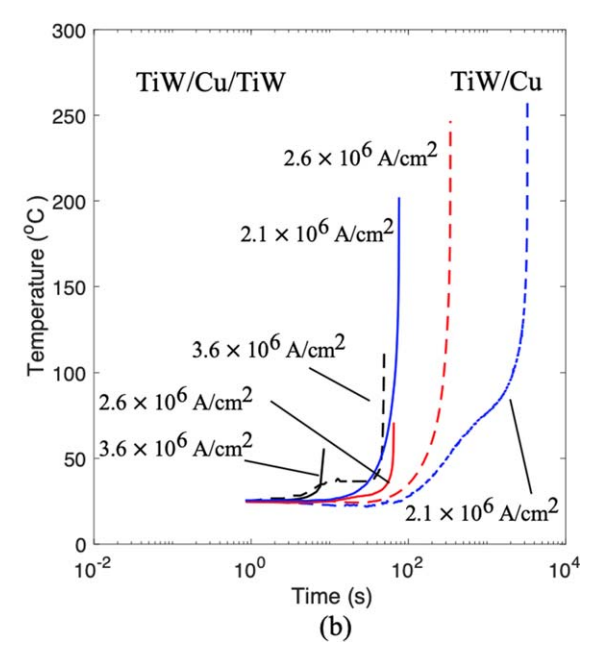
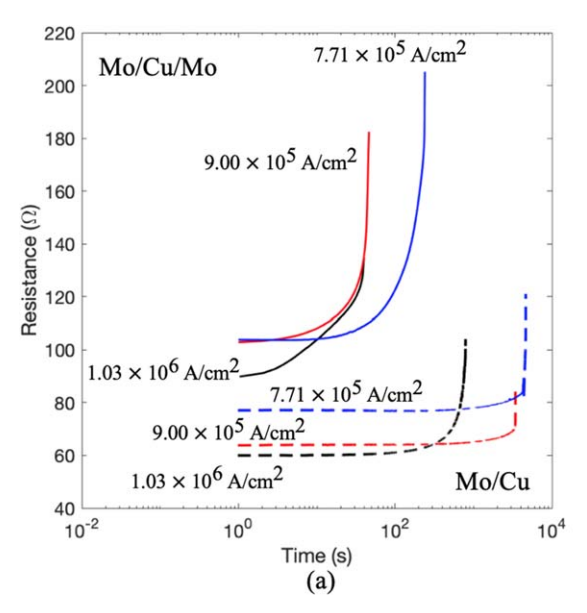


Figure 5. (a) R-t and (b) T-t curves of TiW/Cu and TiW/Cu/TiW lines stressed at  $J = 2.1 \times 10^6$ ,  $2.6 \times 10^6$ , and  $3.6 \times 10^6$  Amp cm $^{-2}$ . Line width (W) 10  $\mu$ m and length (L) 800  $\mu$ m.



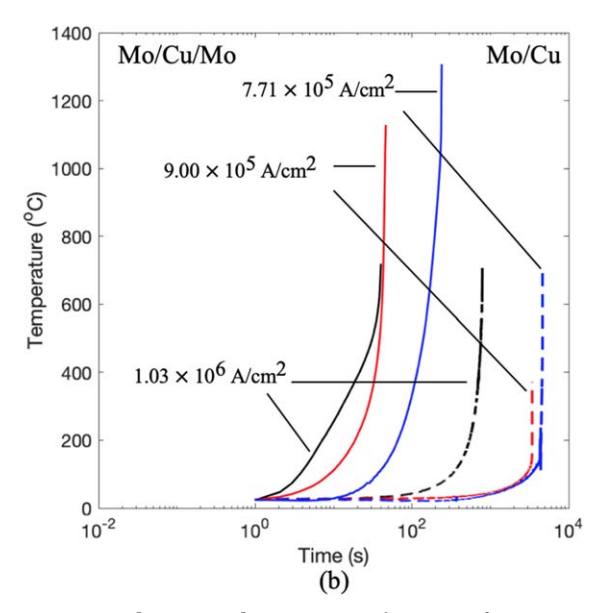
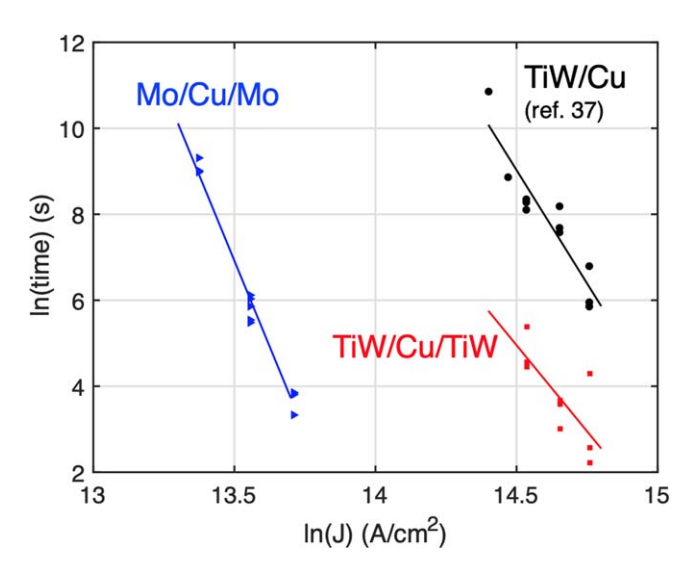


Figure 6. (a) R-t and (b) T-t curves of Mo/Cu and Mo/Cu/Mo lines stressed at  $J = 7.71 \times 10^5$ ,  $9.00 \times 10^5$ , and  $1.03 \times 10^6$  Amp cm $^{-2}$ .  $W = 10 \ \mu m$  and  $L = 800 \ \mu m$ .

700 °C before it was broken, while the temperature of the Mo/Cu/Mo line under the same stress condition was 1300 °C before it was broken. Snice the change of the barrier layer does not influence the line failure mechanism, 57 the above result must be contributed by the Mo capping layer. The addition of the Mo capping layer increased the line resistance because the Mo-Cu bond had a lower conductivity than the Cu-Cu bond had.<sup>58</sup> Slopes of the R-t curves in region 2 of the Mo/Cu/Mo line increase with the stress time while those of the Mo/Cu line are almost independent of the stress time. This phenomenon can be related to the oxidation of the Mo capping layer. The EM stress induced Joule heating led to the increase of temperature, which facilitated the oxidation of the Mo capping layer and therefore, increased the line resistance. 59-65 The slopes of Mo/Cu/Mo lines in region 2 of Figs. 6a and 6b are larger than those of the Mo/Cu lines. The formers are also larger than those of the TiW/Cu/TiW lines in Figs. 5a and 5b. Since the EM stressed Mo/Cu/Mo line has a higher temperature than that of the TiW/Cu/TiW line, the phenomena of capping layer oxidation and the loss of Cu atoms from the bulk Cu layer in the former are more serious than those in the latter. Therefore, the ramp of resistance in region 2 in the former is faster than that in the latter.

Capping layer material and stress current density effects on line breakage time.—Figure 7 shows the lifetimes of TiW/Cu, TiW/Cu/ TiW, and Mo/Cu/Mo lines with respect to the EM stress current density. The black line is the curve of the control sample, i.e., TiW/ Cu without a capping layer.<sup>37</sup> The general trend is that the lifetime decreases with the increase of the current density. 55 Under the same stress condition, the uncapped Cu line has a longer lifetime than the capped Cu line has. The TiW/Cu/TiW line has a longer lifetime than the Mo/Cu/Mo line has. The above phenomenon can be explained by the enhanced void formation from the loss of Cu atoms from the bulk Cu film to the capping layer. It is consistent with the results of Tables I and II. In addition, Figs. 5 and 6 show that the line resistance and temperature of the Mo capped sample are larger than those of the TiW capped sample. Separately, it was reported that TiW has better thermal stability than Mo has. 66 Therefore, it may be easier to form voids in the Mo capped Cu line than in the TiW capped Cu line, which causes the former's shorter lifetime.

Surface color change with stress time.—The color change of the surface with the EM stress time can provide important information on the composition or structure change of the sample. Figure 8a



**Figure 7.** Electromigration failure time of TiW/Cu, TiW/Cu/TiW, and Mo/Cu/Mo lines stressed at different current densities.  $W=10~\mu{\rm m}$  and  $L=800~\mu{\rm m}$ .

shows top views of a TiW/Cu line stressed at  $J = 2.1 \times 10^6$  Amp cm<sup>-2</sup> for different periods of times. The color of the line darkened with the increase of the stress time, which was due to the oxidation of the Cu surface at the raised temperature. 48-52 With the further increase of the stress time, a bright region appeared and the size enlarged. Eventually, the line was broken with the formation of a dark region. Figure 8b shows the color change of a TiW/Cu/TiW line stressed at  $J = 2.1 \times 10^6$  Amp cm<sup>-2</sup> for different periods of times. Originally, the surface showed the purple color that remained the same for a while. As the stress time was increased, the color changed to beige. Eventually, the line was broken with the formation of a dark region. The color change of the TiW capping layer was contributed by two factors: the diffusion of Cu from the bulk Cu layer and the surface oxidation, which was confirmed from the XPS analysis. Since the color change in Fig. 8b occurred in a much shorter period of time than that in Fig. 8a, the TiW capped line has a shorter lifetime than the uncapped Cu line. Independent of the existence or absence of the passivation layer, the line was broken

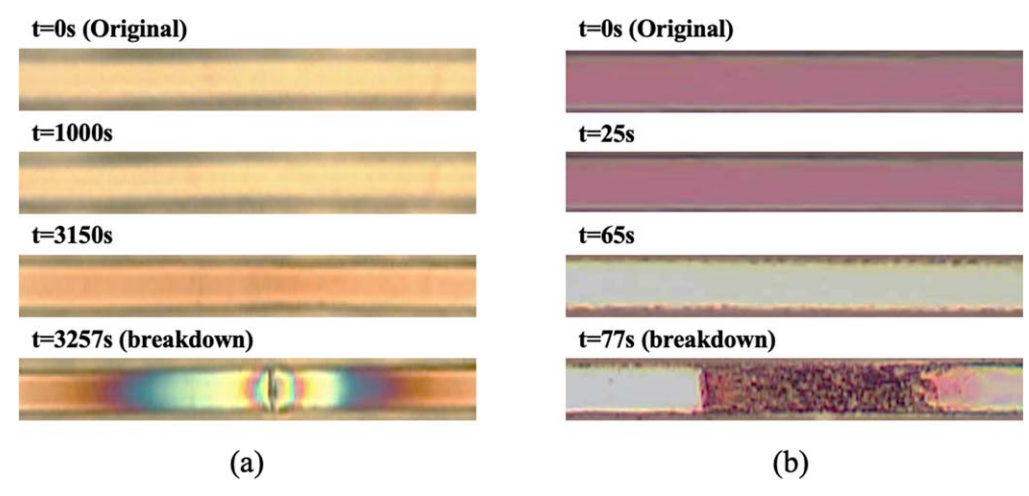


Figure 8. Top views of (a) TiW/Cu and (b) TiW/Cu/TiW lines ( $W = 10 \mu m$ ) stressed at  $J = 2.1 \times 10^6 \text{ Amp cm}^{-2}$ .

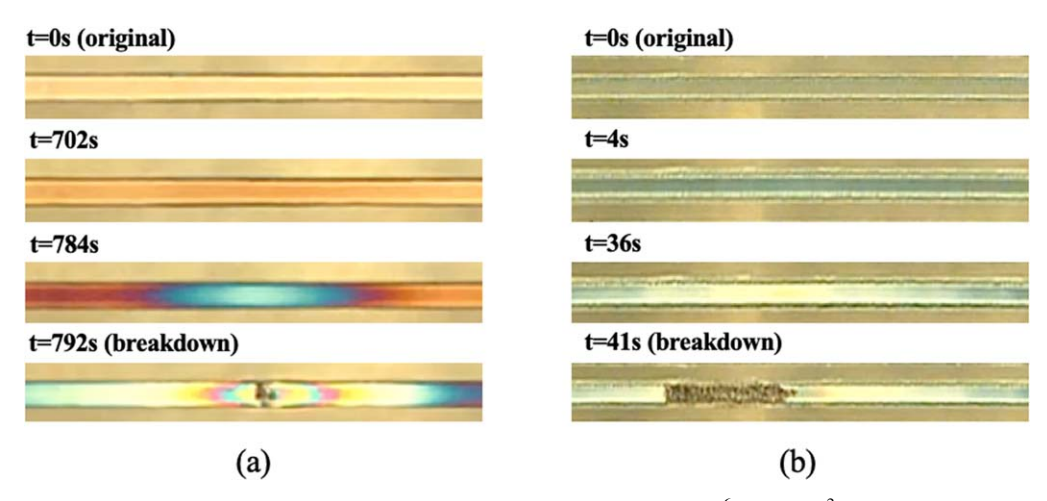


Figure 9. Top views of (a) Mo/Cu and (b) Mo/Cu/Mo lines ( $W = 10 \ \mu \text{m}$ ) stressed at  $J = 1.03 \times 10^6 \ \text{Amp cm}^{-2}$ .

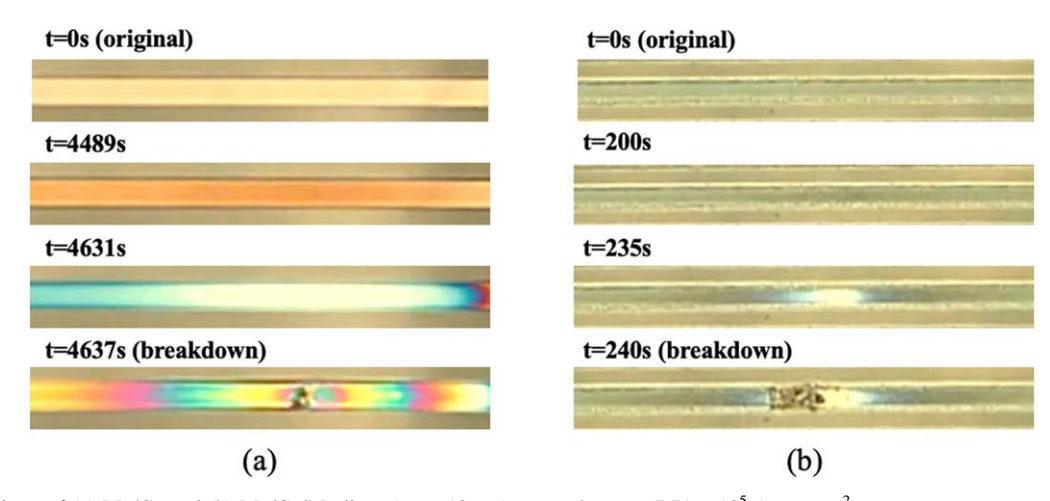


Figure 10. Top views of (a) Mo/Cu and (b) Mo/Cu/Mo lines ( $W = 10 \mu m$ ) stressed at  $J = 7.71 \times 10^5 \text{ Amp cm}^{-2}$ .

about 5 to 10 s after the bright spot appeared, which is consistent with the drastic increase of the line resistance or temperature shown in Figs. 5a and 5b.

The same surface color change with time was observed on the Mo/Cu and Mo/Cu/Mo lines. Figure 9a shows the top views of a Mo/Cu line stressed at  $J = 1.03 \times 10^6$  Amp cm<sup>-2</sup> for different periods of times. In addition to the color change, before the line was

broken, it swelled slightly near the broken point, which can be caused by the high local temperature. Figure 9b shows top views of Mo/Cu/Mo lines stressed at  $J=1.03\times 10^6$  Amp cm $^{-2}$  for different periods of times. The original light green color became darker with the increase of the stress time. A bright region appeared shortly before the line was broken. It changed to a large dark region upon the breakage of the line. The size of the broken spot in the TiW or

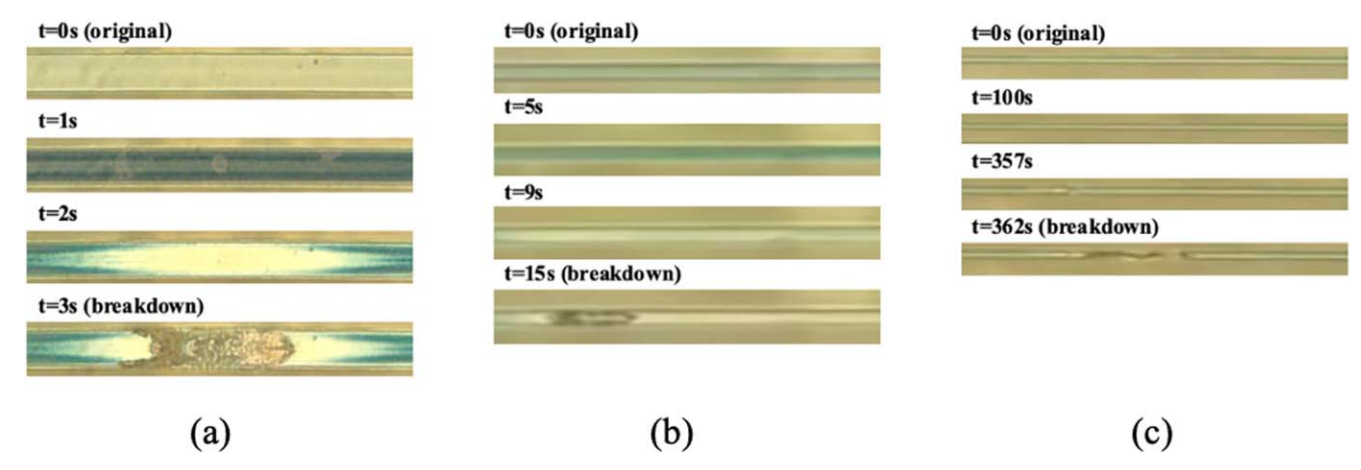


Figure 11. Top views of Mo/Cu/Mo lines at different stress times. (a)  $W = 30 \mu \text{m}$  (b)  $W = 10 \mu \text{m}$  (c)  $W = 2 \mu \text{m}$ .  $J = 1.54 \times 10^6 \text{ Amp cm}^{-2}$ .

Mo capped line was larger than that of the uncapped line, as shown in Figs. 8 and 9. This might be due to the capping layer enhanced Cu diffusion from the bulk Cu film to the capping layer and voids formation at the Cu/capping layer interface. Separately, the trend of color change during EM stress occurred consistently regardless of the magnitude of current density. For example, Fig. 10 shows top views of Mo/Cu and Mo/Cu/Mo lines stressed at a current density about 25% smaller than that of Fig. 9a. The line breakage time of Fig. 10a is 6 times longer than that of Fig. 9a. The color change phenomenon in Fig. 10b is similar to but less obvious than that in Fig. 9b. The longer lifetime and less color change of the line under the low current stress condition than those under the high current stress condition can be contributed by the lower temperature in the former.

Line width effect on surface color change.—The color change during the EM stress was affected by the line width. For example, Fig. 11 shows top views of Mo/Cu/Mo lines of (a) 30  $\mu$ m, (b) 10  $\mu$ m, and (c)  $2 \mu m$  widths stressed at the same current density of J = $1.54 \times 10^6$  Amp cm<sup>-2</sup>. In Fig. 11a, the 30  $\mu$ m wide line changed color with the increase of the stress time obviously. A large bright area where the line eventually broke was observed. When the line width was reduced to 10  $\mu$ m, as shown in Fig. 11b, no obvious timedependent color change was observed. When the line width was further reduced to  $2 \mu m$ , as shown in Fig. 11c, no obvious color change with time was observed until the line was broken. Therefore, the narrower the line is, the less obvious the color change is. This can be explained by the mechanism of voids formation and merging mechanism. <sup>23–25,37,53,54</sup> Figure 12 shows schematic diagrams of grain boundary distributions in lines of different widths. Under the same deposition condition, grains of the same size are uniformly distributed across the line independent of the line width.<sup>67</sup> The narrow line has fewer grain boundaries to initiate voids formation than the wide line has. Therefore, voids are easier to form in the wide line than in the narrow line to cause the quicker breakage of the former.

Passivation layer effect on line failure mechanism.—The EM stress result shows that the addition of a TiW or Mo capping layer shortens the lifetime although shapes of their *R-t* curves are similar. The TiW and Mo capped Cu lines have higher temperatures than that of the uncapped Cu lines. There are several possible causes for this result. For example, the TiW and Mo films have lower thermal conductivities than the Cu film has. <sup>52,68–70</sup> This kind of passivation layer hinders the dissipation of Joule heat during the EM stress, which leads to the higher temperature. Separately, the XPS result showed that Cu atoms were diffused to the capping layer during the EM stress, which accelerated the line breakage process. Therefore, the EM failure mechanism of a capped Cu line can be outlined as shown in Fig. 13. It is composed of 4 steps: voids formation at joints

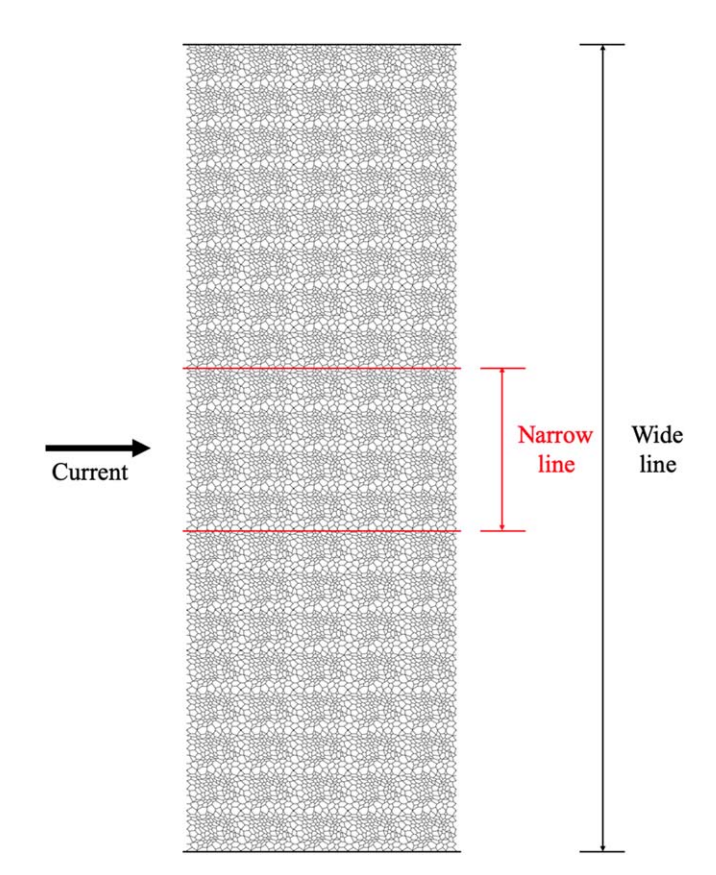


Figure 12. Schematic of the grain boundaries in narrow and wide interconnection Cu lines.

of grain boundaries, enhanced voids formation from Cu diffusion to the capping layer, the merge of voids, and the connection of voids to form the line broken region. Although the capping layer can prevent the Cu layer from oxidation in air or reaction with the adjacent film, it could accelerate the formation of voids in the second step, which shortens the lifetime of the Cu stack.

### Conclusions

The EM failure phenomena of the TiW/Cu, TiW/Cu/TiW, Mo/Cu, and Mo/Cu/Mo lines etched from a plasma-based process on glass substrate were investigated. The time-dependent changes of line resistance were measured, which were used to estimate the temperature changes assuming negligible heat dissipation through the glass substrate. Although the capping layer could protect the Cu

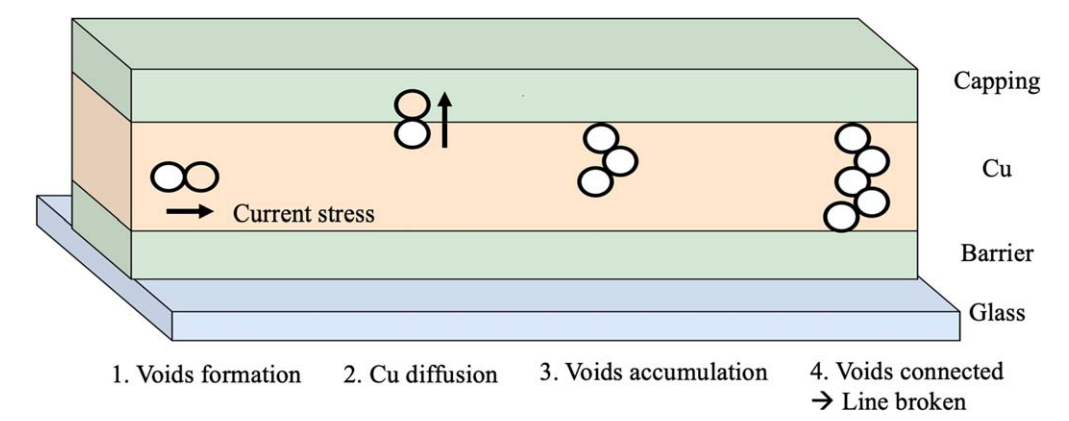


Figure 13. Schematic of the line failure mechanism model of the plasma etched Cu lines with passivation layer under electromigration stress.

line from oxidation in air, it shortened the lifetime. The sample with the capping layer has a higher temperature than that without the capping layer because of the less effective heat dissipation, which induced the loss of Cu atoms and enhanced voids formation and growth in the bulk Cu layer. The above process is less serious in the TiW capped line than in the Mo capped line, which is supported by the XPS analysis, time dependent temperature, and line breakage time. Changes of color and shapes of the sample along the EM stress time were consistent with variations of composition and electrical property. A 4-step mechanism of the failure of the capped Cu line has been presented based on the above result. In summary, the addition of a capping layer can protect the Cu line from environment contamination but at the same time shortens the lifetime. The capping layer material is critical to the lifetime of the Cu line.

# Acknowledgments

Authors acknowledge the support of this work by NSF CMMI 1633580 project. Part of the content of this paper was presented in the 235th ECS Meeting in Dallas, TX, USA, May 2019, the International Conference on Semiconductor Technology for Ultra Large Scale Integrated Circuits and Thin Film Transistors (ULSIC vs TFT 7) in Kyoto, Japan, May 2019 and the 236th ECS Meeting in Atlanta, GA, USA, October 2019, and was published in the ECS Transactions 89(3), 87–92 (2019), the ECS Transactions 90(1), 65-72 (2019), the ECS Transactions 92(5), 9-16 (2019), and the ECS Transactions 92(5), 39-46 (2019).

#### ORCID

Jia Quan Su https://orcid.org/0000-0001-8200-8695 Minggian Li https://orcid.org/0000-0002-5177-7341 Yue Kuo https://orcid.org/0000-0003-2757-1842

# References

- 1. National Technology Roadmap for Semiconductors (NTRS), SIA (1997).
- 2. Y. Kuo, ECS Interface, 22, 55 (2013).
- 3. J. Proost, T. Hirato, T. Furuhara, K. Maex, and J.-P. Celis, J. Appl. Phys., 87, 2792
- 4. C. S. Hau-Riege, S. P. Hau-Riege, and A. P. Marathe, J. Appl. Phys., 96, 5792 (2004).
- 5. C. Yu, P. C. Fazan, V. K. Mathews, and T. T. Doan, Appl. Phys. Lett., 61, 1344 (1992).
- 6. M. Fayolle and F. Romagna, Microelectronic Eng., 37, 135 (1997).
- 7. R. Chang, Y. Cao, and C. J. Spanos, IEEE Trans. on Electron Dev., 51, 1577 (2004).
- Y. Kuo and J. R. Crowe, J. Vac. Sci. Technol. A, 8, 1529 (1990).
- 9. P. E. Riley, J. Electrochem. Soc., 140, 1518 (1993).
- 10. D. A. Danner, M. Dalvie, and D. W. Hess, J. Electrochem. Soc., 134, 669 (1987).
- 11. P. M. Schaible, W. C. Metzger, and J. P. Anderson, J. Vac. Sci. Technol., 15, 334 (1978).
- 12. D. J. Cooperberg, V. Vahedi, and R. A. Gottscho, J. Vac. Sci. Technol. A, 20, 1536
- 13. H. Miyazaki, K. Takeda, N. Sakuma, S. Kondo, Y. Homma, and K. Hinode, J. Vac. Sci. Technol. B, 15, 237 (1997).

- 14. Y. Kuo and S. Lee, Japan J. Appl. Phys., 39, L188 (2000).
- 15. S. Lee and Y. Kuo, J. Electrochem. Soc., 148, G524 (2001).
- 16. Y. Kuo and S. Lee, Appl. Phys. Lett., 78, 1002 (2001).
- 17. S. Lee and Y. Kuo, Japan J. of Appl. Phys., 41, 7345 (2002).
- 18. Y. Kuo, AVS 65th Intl. Symp. & Exhib., Abst. #1108, Long Beach, CA, Oct. 21-26 (2018).
- 19. Y. Kuo, Proc. 6th Intl. Conf. Reactive Plasmas & 23rd Symp. Plasma Processing, 29-30 (2006).
- 20. Y. Kuo, H. Nominanda, and G. Liu, J. Korean Phys. Soc., 48, S92 (2006).
- 21. J. Yang, Y. Ahn, J. Bang, W. Ryu, J. Kim, J. Kang, M. S. Yang, I. Kang, and I. Cung, ECS Trans., 16, 13 (2008).
- 22. P. A. Tamirisa, G. Levitin, N. S. Kulkarni, and D. W. Hess, Microelectron. Eng., 84, 105 (2007).
- 23. C. S. Hau-Riege, Microelectron. Reliab., 44, 195 (2004).
- 24. G. Liu and Y. Kuo, J. Electrochem. Soc., 156, H579 (2009).
- 25. M. Li and Y. Kuo, ECS Trans., 86, 41 (2018).
- 26. C. Ryu, H. Lee, K.-W. Kwon, A. L. S. Loke, and S. S. Wong, Solid State Technol., 42, 53 (1999).
- S. Song, Y. Liu, D. Mao, H. Ling, and M. Li, *Thin Solid Films*, **476**, 142 (2005).
   J.-C. Chuang, S.-L. Tu, and M.-C. Chen, *Thin Solid Films*, **346**, 299 (1999).
- 29. G. Liu and Y. Kuo, J. Electrochem. Soc., 154, H653 (2007).
- 30. Y. Kuo, J. Electrochem. Soc., 137, 1907 (1990).
- 31. S. M. Rossnagel and T. S. Kuan, J. Vac. Sci. Technol. B, 22, 240 (2004).
- 32. S. Jeong, K. Woo, D. Kim, S. Lim, J. S. Kim, H. Shin, Y. Xia, and J. Moon, Adv. Funct. Mater., 18, 679 (2008).
- 33. A. Yabuki and S. Tanaka, Mater. Res. Bull., 46, 2323 (2011).
- 34. C.-K. Hu, L. Gignac, R. Rosenberg, E. Liniger, J. Rubino, C. Sambucetti, A. Domenicucci, X. Chen, and A. K. Stamper, Appl. Phys. Lett., 81, 1782 (2002).
- 35. C.-K. Hu, L. Gignac, R. Rosenberg, E. Liniger, J. Rubino, C. Sambucetti, A. Stamper, A. Domenicucci, and X. Chen, Microelectronic Eng., 70, 406
- 36. S. Yokogawa and Y. Kakuhara, Japan J. of Appl. Phys., 50, 05EA02 (2011).
- 37. M. Li, J. Q. Su, and Y. Kuo, ECS Trans., 89, 87 (2019).
- 38. L. D. Hartsough, *Thin Solid Films*, **64**, 17 (1979).
- 39. J. S. H. Cho, H.-K. Kang, S. S. Wong, and Y. Shacham-Diamand, MRS Bull., 18, 31 (1993).
- 40. A. Marcelli et al., *Surf. Coat. Tech.*, **261**, 391 (2015).
  41. EIA/JESD33-B, "Standard method of measuring and using the temperature coefficient of resistance to determine the temperature of a metallization line." (2004)
- 42. S. W. Goh, A. N. Buckley, R. N. Lamb, R. A. Rosenberg, and D. Moran, Geochim. Cosmochim. Acta, 70, 2210 (2006).
- M. C. Biesinger, L. W. M. Lau, A. R. Gerson, and R. S. C. Smart, Appl. Surface Science, 257, 887 (2010).
- 44. S. Poulston, P. M. Parlett, P. Stone, and M. Bowker, Surf. Interface Anal., 24, 811 (1996).
- 45. L. Meda and G. F. Cerofolini, Surf. Interface Anal., 36, 756 (2004).
- 46. F. Li, L. Zhang, D. G. Evans, and X. Duan, Colloid Surface A, 244, 169 (2004).
- 47. R. A. Isaacs, H. M. I. Jaim, D. P. Cole, K. Gaskell, O. Rabin, and L. G. Salamanca-Riba, Carbon, 122, 336 (2017).
- Y. S. Gong, C. Lee, and C. K. Yang, J. Appl. Phys., 77, 5422 (1995).
- 49. K. Hinode, Y. Hanaoka, K. Takeda, and S. Kondo, Japan J. of Appl. Phys., 40, L1097 (2001)
- 50. C. N. Hinshelwood, Proceedings of the Royal Society of London, Series A, 102, 318 (1922).
- 51. M. Momcilovic, M. Trtica, J. Ciganovic, J. Savovic, J. Stasic, and M. Kuzmanovic, Appl. Surf. Sci., 270, 486 (2013).
- 52. P. Nath and K. L. Chopra, Thin Solid Films, 20, 53 (1974).
- 53. C.-K. Hu, L. Gignac, and R. Rosenberg, Microelectron. Reliab., 46, 213 (2006).
- 54. C.-C. Lin and Y. Kuo, MRS Online Proceedings Library Archive, 1428 (2012). 55. J. R. Black, IEEE Trans., 16, 338 (1969).
- 56. J. W. Nah, J. O. Suh, and K. N. Tu, J. Appl. Phys., 98, 013715 (2005).
- 57. M. Li, J. Q. Su, and Y. Kuo, ECS Trans., 92, 9 (2019).

- 58. M. W. Lane, E. G. Liniger, and J. R. Lloyd, *J. Appl. Phys.*, **93**, 1417 (2003). 59. H. J. Grabke and G. H. Meier, *Oxid. Met.*, **44**, 147 (1995).
- 60. E. A. Gulbransen, K. F. Andrew, and F. A. Brassart, *J. Electrochem. Soc.*, **110**, 952 (1963).
- 61. E. S. Jones, C. J. F. Mosher, R. Speiser, and J. W. Spretnak, *Corrosion*, 14, 20 (1958).
- N. Floquet, O. Bertrand, and J. J. Heizmann, Oxid. Met., 37, 253 (1992).
   L. Wang, G.-H. Zhang, and K.-C. Chou, J. Refractory Metals and Hard Materials, **57**, 115 (2016).
- 64. L. Brewer and R. H. Lamoreaux, J. Phase Equil., 1, 85 (1980).

- 65. M. Arita, H. Kaji, T. Fujii, and Y. Takahashi, *Thin Solid Films*, 520, 4762 (2012). 66. V. G. Glebovsky, V. Y. Yaschak, V. V. Baranov, and E. L. Sackovich, *Thin Solid*
- Films, 257, 1 (1995).
- G. Liu, Y. Kuo, S. Ahmed, D. N. Buckley, and T. Tanaka-Ahmed, *J. Electrochem. Soc.*, 155, H432 (2008).
- R. D. Allen, L. F. Glasier Jr., and P. L. Jordan, *J. Appl. Phys.*, 31, 1382 (1960).
   M. Yi, H. V. Panchawagh, R. J. Podhajsky, and R. L. Mahajan, *IEEE Trans. On*
- Biomed. Eng., **56**, 2477 (2009).

  70. K. L. Grosse, F. Xiong, S. Hong, W. P. King, and E. Pop, *Appl. Phys. Lett.*, **102**, 193503 (2013).